A New Inspection Method for a EUV Mask Defect Inspection System

Ding Qi[1], Kuen-Yu Tsai*[1], Jia-Han Li[2]

[1]Department of Electrical Engineering
[2]Department of Engineering Science and Ocean

National Taiwan University
Taipei, Taiwan

2014/6/26

Outline

1. Motivation
2. Introduction
   a) Non-actinic EUV Mask Defect Inspection
   b) Previous Actinic Inspection Techniques
   c) Problem Statements
3. A New Inspection Method
   a) Defect Feature Parameterization
   b) Inspection Strategy
   c) Defect Size Estimation with noise-free detectors
4. Photon Shot Noise and Countermeasures
5. Defect Location Determination Difficulty and Countermeasures
6. Conclusion
7. References

Motivation

- Printable-defect-free EUV mask one major EUVL challenge
- EUV mask defect inspection a critical item in ITRS[1]

Table LITH2 Lithography Difficult Challenges

	Near Term Challenges (2013–2016)
1	Cost and cycle time of multiple patterning – especially for more than 2x
2	Process control on key parameters such as overlay, CD control, LWR with multiple patterning
3	EUV Source power
4	EUV Mask Infrastructure (defect inspection and verification, mitigation, mask lifetime) Defect free EUV mask blanks, mask availability
5	EUV resist and/or process that meets sensitivity, resolution, LER requirements
6	DSA defectivity and positional accuracy

Non-actinic (Blue/DUV) EUV Mask Defect Inspection

- Non-actinic inspection tools:
  - e.g., confocal microscope, Lasertec M1350 & M7360, λ = 488, 266 nm
  - collaborative efforts (Intel/Sematech/LBNL…) in 2000s[17] 2005, Intel
- Detection limits on multilayer (ML) blanks:
  - M1350: ~70 nm, capture rate ~100%
  - M7360: ~40 nm, capture rate ~95.2%[2] 2014, Sematech
  - insufficient for critical layers beyond 22 nm half-pitch ("10 nm") node
- Light-intensity penetration[3] 2007, LBNL

λ	*R*	1% depth	bi-layers
13.4 nm	72.7%	215 nm	31
488 nm	58.4%	53.6 nm	8
266 nm	41.9%	20.6 nm	3

  - only "skin-deep" multilayer information
  - e.g. may miss printable defects at deeper levels with "defect smoothing" ML coating processes

Previous Actinic Inspection Techniques

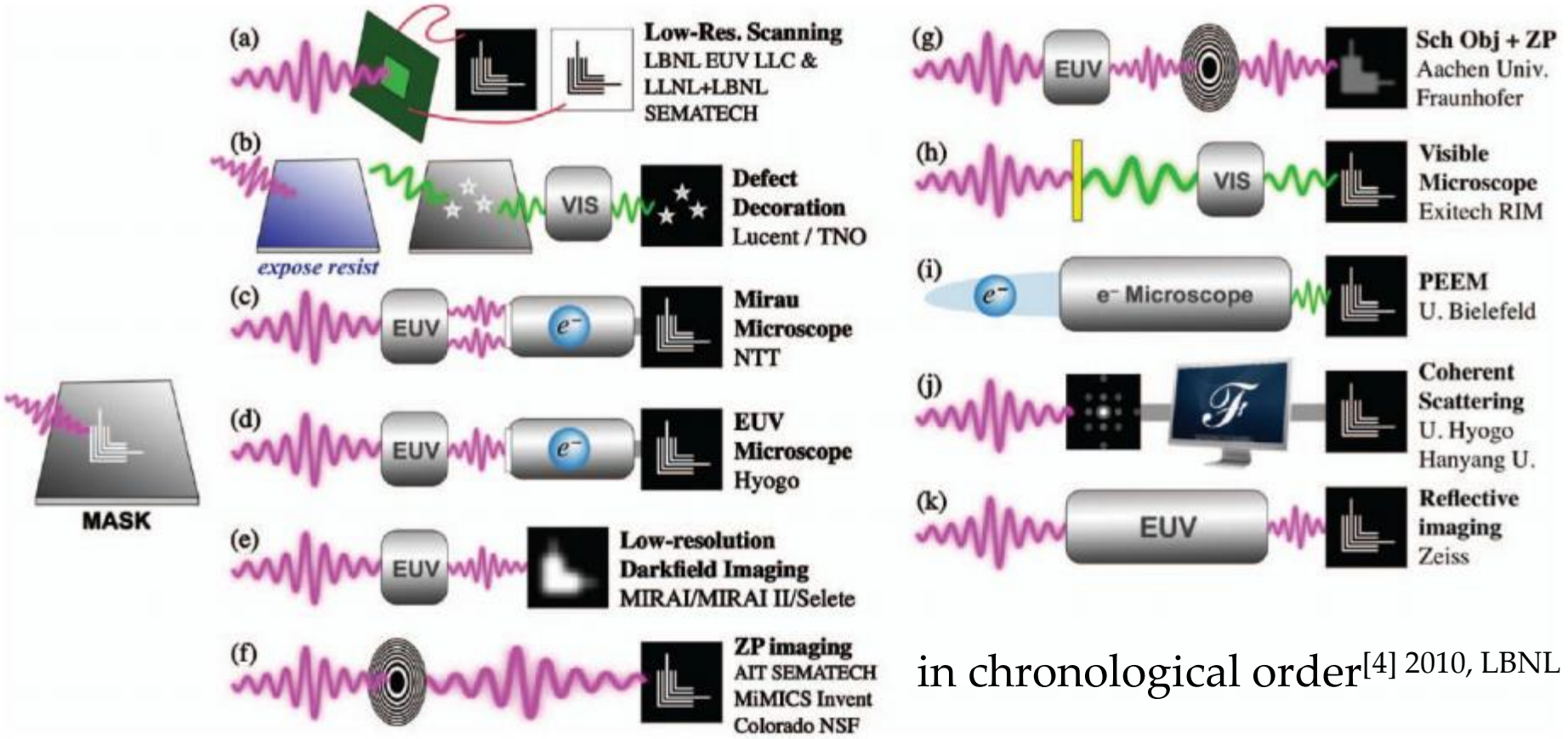

in chronological order[4] 2010, LBNL

(l) The SEMATECH High Numerical Aperture Actinic Reticle Review Project (SHARP), 2013, successor of AIT (f)[5] 2013, LBNL/Sematech

(m) Lasertec Actinic Blank Inspection (ABI) tool: based on (e)[6] 2013, Lasertec

(n) Reflective EUV Mask Scanning Lensless Imaging Tool (RESCAN) in Switzerland, 2014, similar with (j)[7]2014, Paul Scherrer Institut (Switzerland)

Coherent Scatterometry Microscopy with Coherent Diffraction Imaging (CDI)

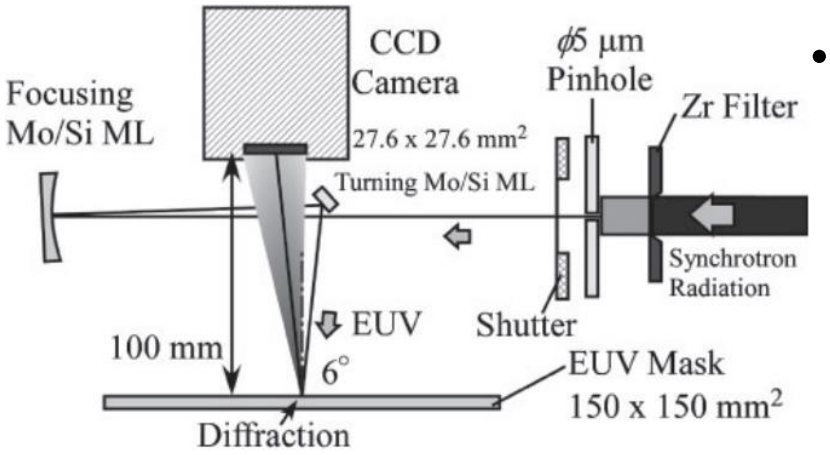

[8] 2009, Univ. Hyogo

- Optics breakthrough, requiring minimum optical hardware
  - no difficult high NA ML/ZP lens
  - resolution limited by detector array/pixel sizes
  - detectors only intensity dist.; phase info. lost
- Bottleneck: phase retrieval computational efforts
  - a hybrid-input-output (HIO) algorithm: large reconstruction error
  - ptychographical CDI: requires much effort on probe information[9],[10] 2011, Univ. Hyogo
  - Typically requiring more than several hundred iterations
  - demonstrated reso.: 25/1.4 nm wide/depth
- Computation complexity origin: a large number of unknowns (e.g., phase of each pixel)

Problem Statements

- Practical industry needs from defect *inspection*:
  - detecting critical-defect existence
  - number of defects and locations
  - defect size good to know, details from defect *review* (e.g., AFM/SEM)

Year of Production	2013	2014	2015	2016	2017	2018	2019	2020
LITH2-Requirements								
DRAM ½ minimum pitch (nm)	28	26	24	22	20	18	17	15
EUVL-specific Mask Requirements								
Substrate defect size (nm) [L]	20	20	20	20	20	20	20	20
Blank defect size (nm) [M]	23	21	19	17	16	15	27	25

- Historically, *imaging* resolution always identified the key inspection bottleneck
  - Hardware-based *imaging*: significant optics cost at high NA
  - Software-based *imaging*: significant computational time/cost
    - CDI still an *imaging* concept, replacing imaging lenses with software lenses

Why worrying so much about defect *imaging* in defect *inspection*?

"Hey, you got something on your nose…"

– That's enough for "inspection".

Problem Reformulation

- Objectives of defect *inspection*:
  - judging defect *existence*
  - detecting *sufficient* defect *features* (e.g., location, shape, size… whichever necessary for yield control)
- Remaining defect *imaging* details left to defect *review* in defect root cause analysis
- NTU proposes a new lens-less, non-imaging defect *inspection* method/concept based on defect *feature estimation* from scattering signals
  - only a small number of unknowns

patent pending

Defect Feature Parameterization (1/2)

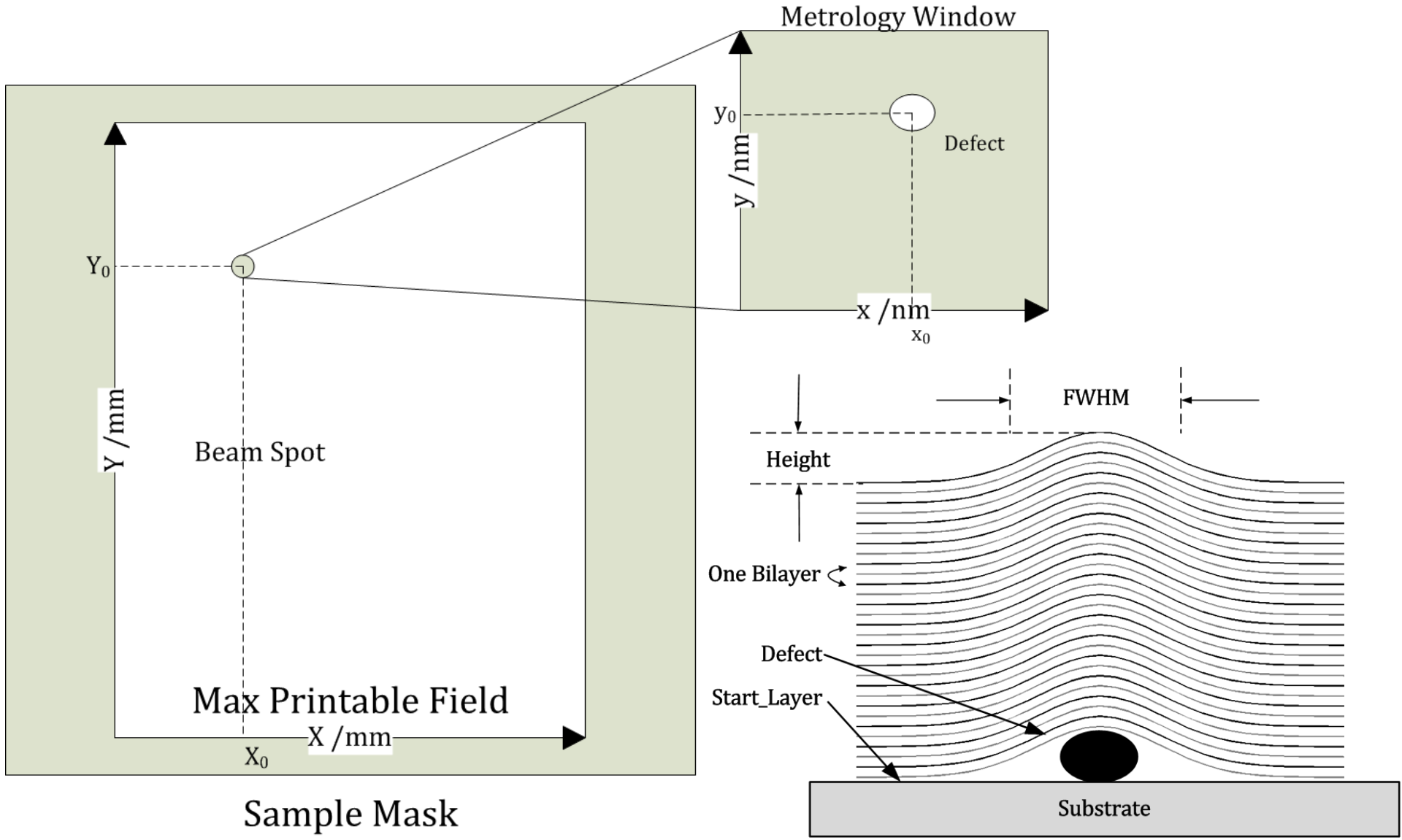

Defect Parameterization (2/2)

Exemplary Feature Parameter List:

Region	Feature	Parameter
Scan Area	Beam Spot Location	X_0 Y_0
Within Beam Spot (Computational Metrology Window)	Defect Location within Beam Spot	x_0 y_0
	Gaussian-Shape Defect Size	FWHM_x FWHM_y Height
	Depth	Start_layer
⋮		

A (Similar) Coherent Diffraction Defect Review/Inspection Hardware

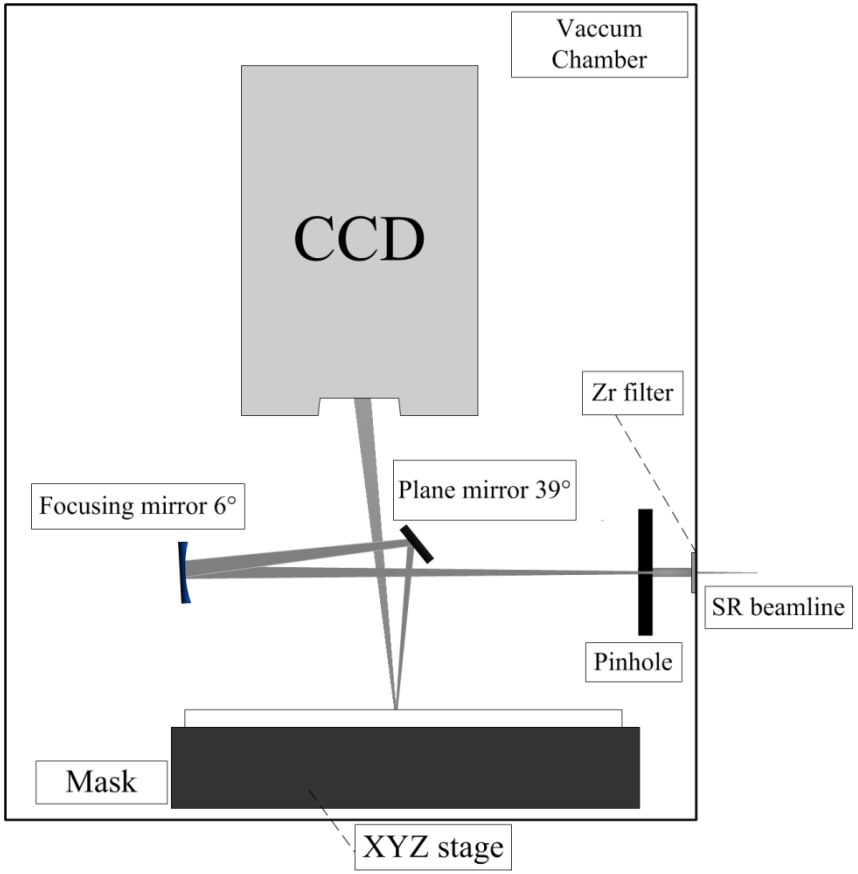

Optics Layout

- Source: NSRRC EUV beamline
- CCD output: Scattered diffraction image
- XYZ stage: calibration and mask scan supported
- Inspection object: currently EUV ML mask blanks

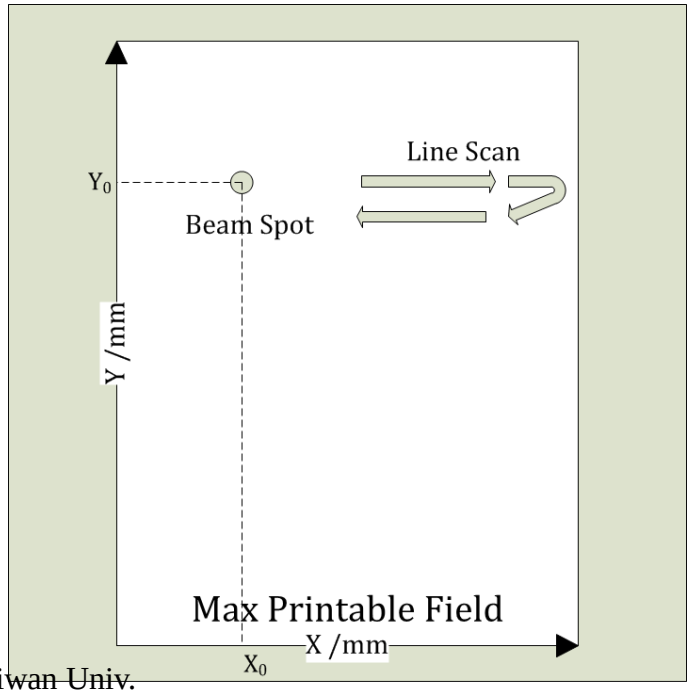

Sample Mask

Inspection Strategy (1/2)

- Fast scan for suspicious spots
  - Spot Size: Ø = 5 micron
  - Step scan, based on a shot-to-shot comparison
  - Suspicious location judged by the deviation (e.g. normalized mean-square error (NMSE)) in diffraction signals (usually matrices) from ideal

$$\mathrm{NMSE}(\mathbf{A},\mathbf{B}) \triangleq \frac{\sum_{i=1}^{n} |a_i - b_i|^2}{\sum_{i=1}^{n} |b_i|^2}$$

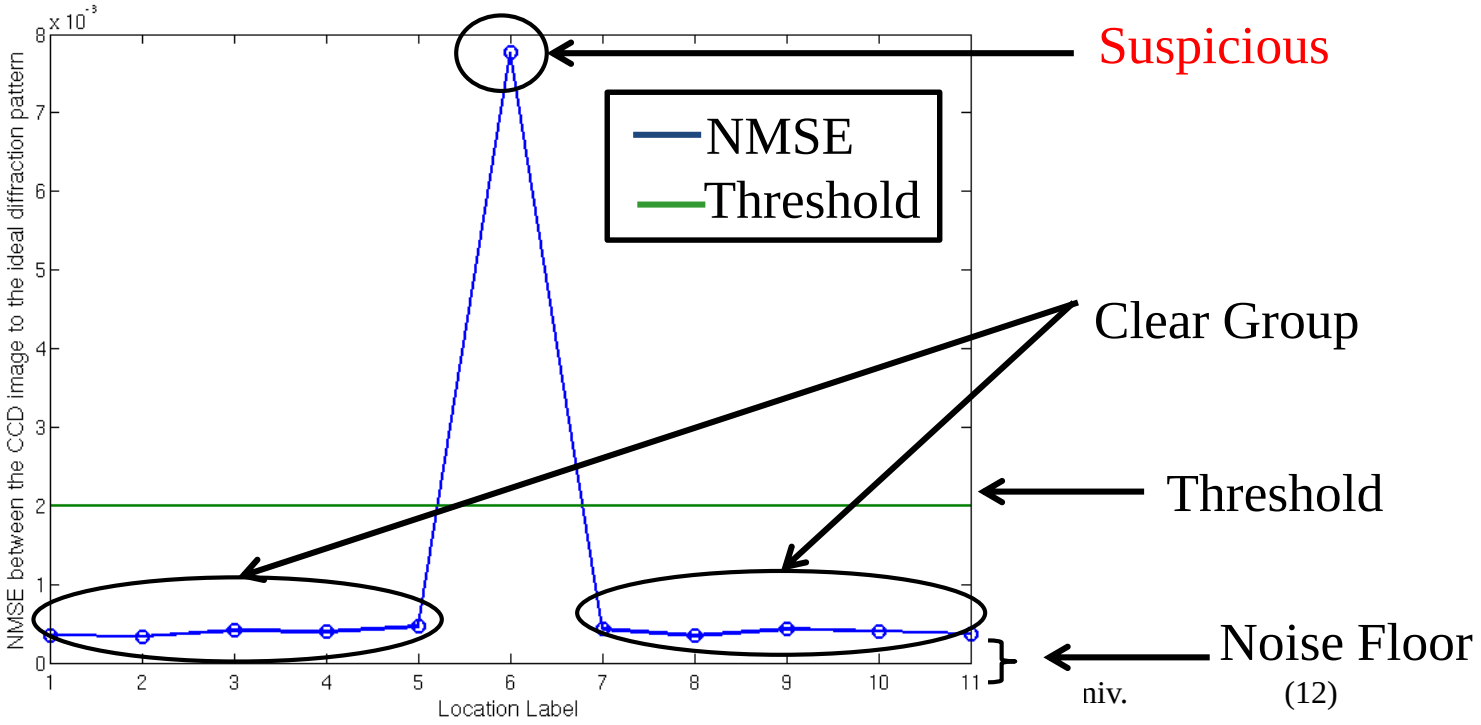

Inspection Strategy (2/2)

- Defect *feature estimation*
  - A non-imaging technique with defect parameterization, defect scattering (optional: ML growth) simulation and mathematical optimization
  - Target: Detect defect *features* (rather than *image reconstruction*)
  - A generic defect feature parameter estimation algorithm
    - ① Initialization: Obtaining actual diffraction signals and create a hypothetic defect
    - ② Iteration: Simulating its diffraction signals,
    - ③ Calculating their differences (e.g. NMSE),
    - ④ Reducing difference by *adjusting hypothetic defect feature* parameter values
    - ⑤ Output: converged defect feature parameters

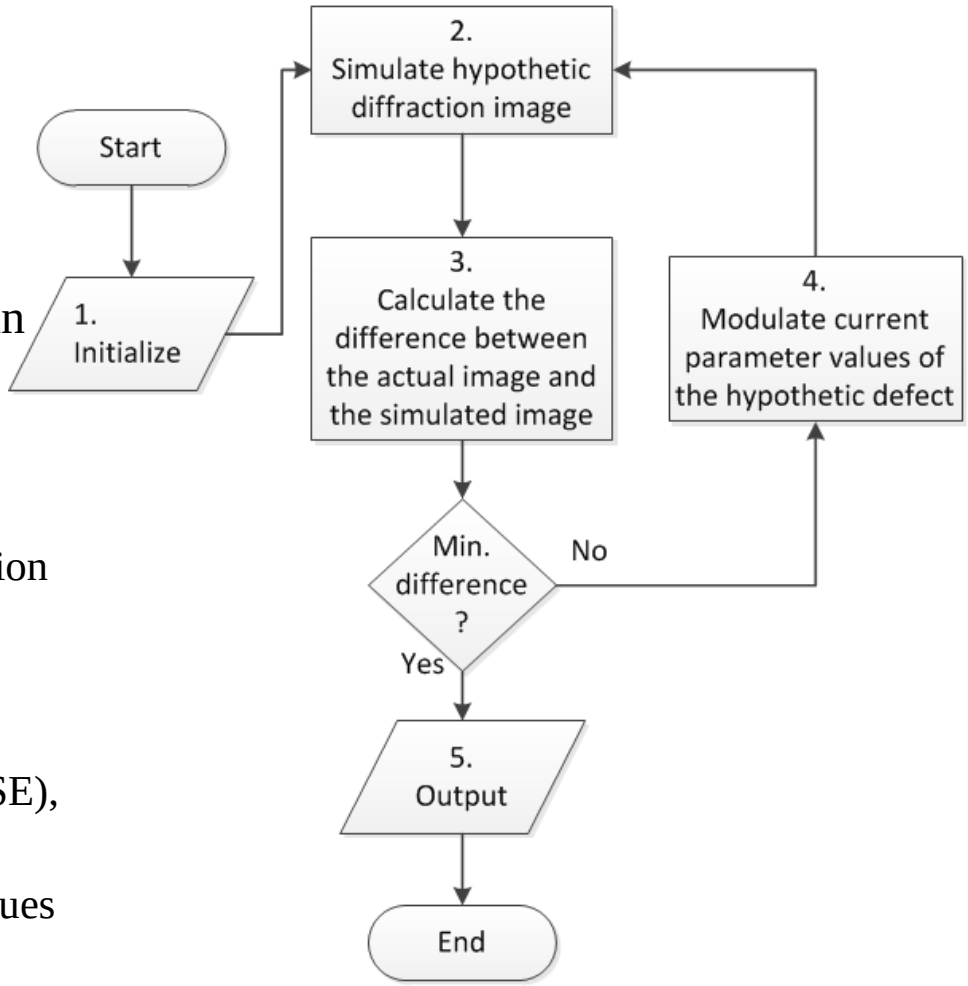

Demonstration: Gaussian Defect Size Estimation, noise-free detectors

- Programmed Defect Parameters:
  - FWHM_x = 10 nm
  - FWHM_y = 10 nm
  - height = 1.5 nm
- Scattering Model: Single Surface Approximation (SSA)[11] 2002, LBNL
- Optimization Tool: Matlab Optimization Toolbox
- Optimization algorithm: *fmincon*
- Optimization cost function:

$$\min . J(x) \triangleq \mathrm{NMSE}(\mathbf{S}(x), \mathbf{C})$$

$$\text{subj. } x \geq [0\ 0\ 0]$$

$$\text{where } x \triangleq [x_{\mathrm{FWHM}}\ \ y_{\mathrm{FWHM}}\ \ h]$$

$\mathbf{S}(x) \in \mathbf{R}^{n \times n}$: simulated diffraction signals

$\mathbf{C} \in \mathbf{R}^{n \times n}$: captured diffraction signals

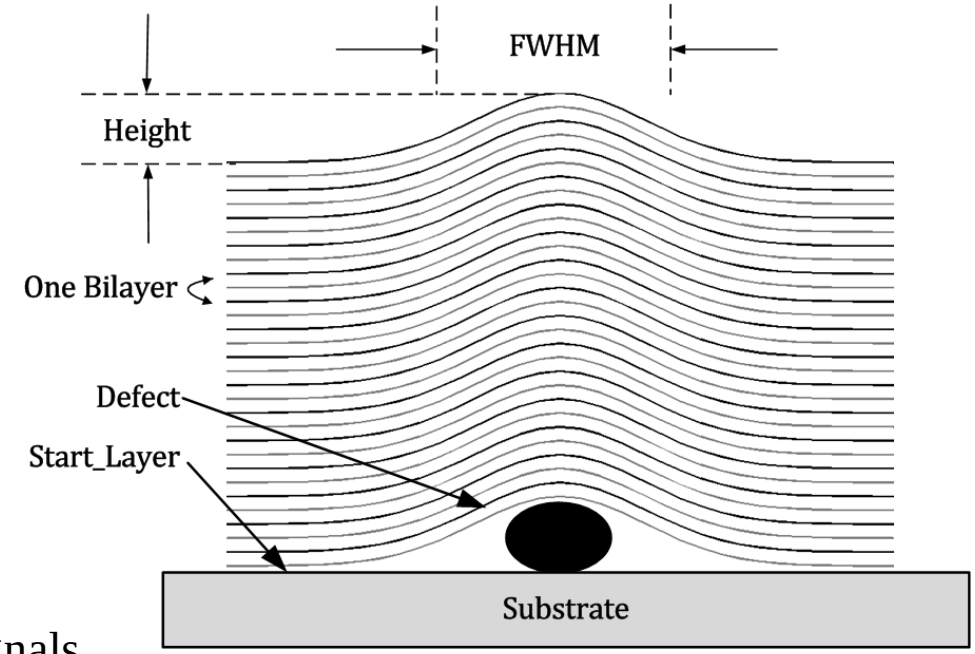

Convergence of estimation errors

Scattering signal target

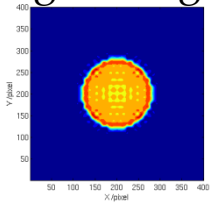

Iteration 1 Iteration 3 Iteration 5 Iteration 7 Iteration 9 Iteration 11 Iteration 13

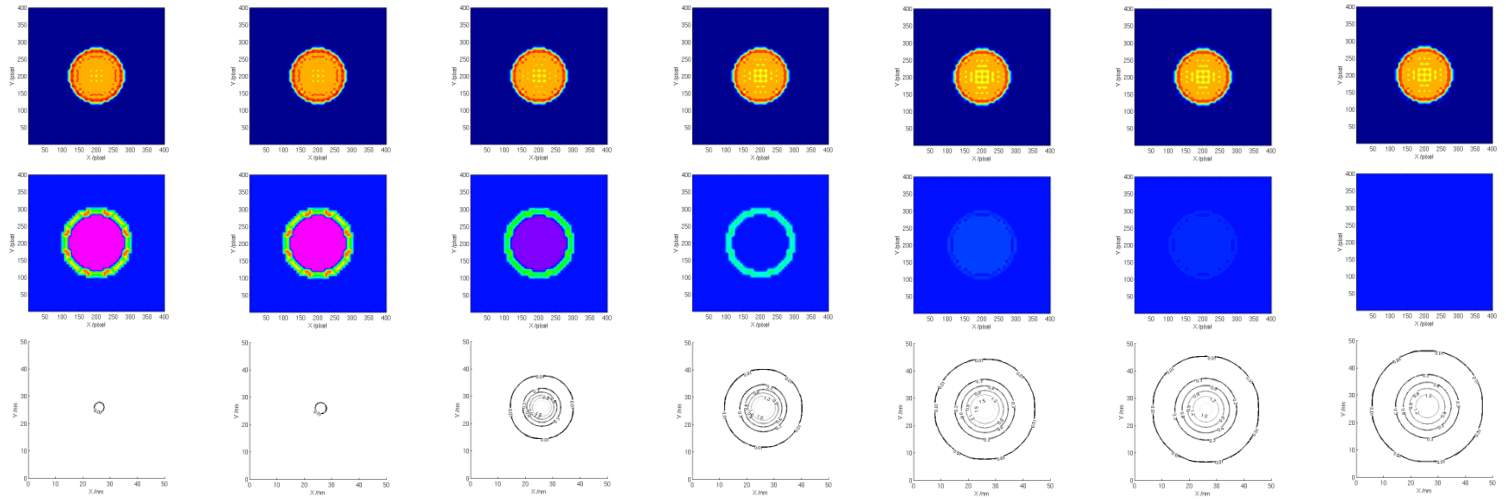

Error→

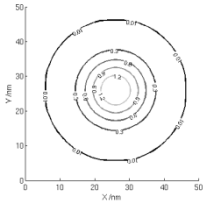

↑Hypothetic defect topography

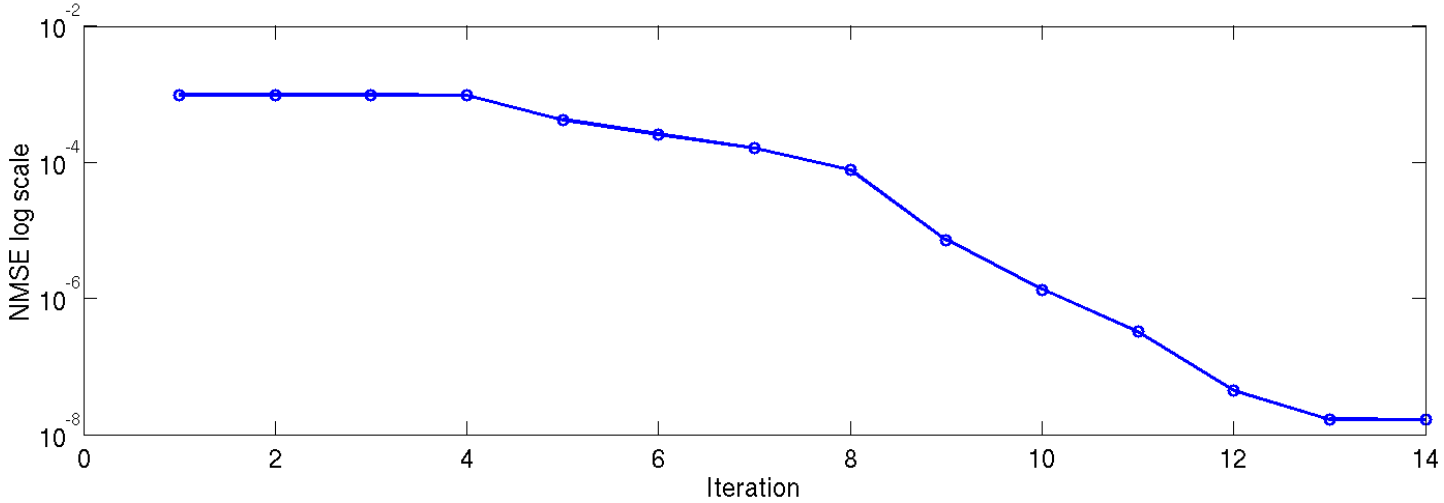

Size Estimation Results (noise-free detectors)

	2015 (22 nm node)	2018 (16 nm node)	2021 (11 nm node)
Target FWHM_x,y	10 nm	7 nm	4 nm
Estimated FWHM_x	10.0506 nm	7.0343 nm	4.0405 nm
Estimated FWHM_y	10.0472 nm	7.0318 nm	4.0360 nm
Target height	1.5 nm	1 nm	0.5 nm
Estimated height	1.4889 nm	0.9931 nm	0.4894 nm
Relative error	0.57%	3.38%	1.34%
Number of iterations	14	16	11
Num. function evaluations	129	147	107
Computation time*	0.43 hour	0.49 hour	0.357 hour

*Computation environment: Intel Xeon E5520 ×2 @2.27 Ghz, 96G DDR3 RAM

Photon Shot Noise and Countermeasures

- Consequence of quantum discretization
- Flux of photon ↓, photon shot noise ↑.[12] 2010, LBNL
- Can be modeled with Poisson Distribution.
  - $\lambda = \bar{n}$ (average detectable photon number).
  - Signal-to-noise ratio (SNR) = $\sqrt{\bar{n}}$.

- Influence to the feature estimation algorithm:
  - Defect parameter values can drift after optimization reaches noise floor

- Possible Solution:
  - Statistical averaging (repeated estimations for averaging)
  - Increase SNR (better detector hardware)

Demonstration: Size Estimation Results (detector SNR = 20, different averaging numbers)

Number of averaging	10 times	20 times	30 times
Target FWHM_x,y	10 nm	10 nm	10 nm
Mean Value of FWHM_x	12.8405 nm	12.0726 nm	11.6426 nm
Standard Deviation of FWHM_x	2.7858 nm	2.8142 nm	2.7713 nm
Mean Value of FWHM_y	11.2104 nm	11.6268 nm	11.5260 nm
Standard Deviation of FWHM_y	2.4025 nm	2.1136 nm	2.3092 nm
Target height	1.5 nm	1.5 nm	1.5 nm
Mean Value of height	1.1493 nm	1.1732 nm	1.2244 nm
Standard Deviation of h	0.2664 nm	0.2375 nm	0.2338 nm
Relative error	21.3%	19.6%	16.7%

- Possible Solution:
  - Statistical averaging √ (more computational cost)
  - Increase SNR

Demonstration: Size Estimation Results (different detector SNRs, ave. number = 30) (1/2)

	SNR=20	SNR=40	SNR=60	SNR=80	SNR=100
Preset of FWHM_x,y	10 nm	10 nm	10 nm	10 nm	10 nm
Mean Value of FWHM_x	11.6426 nm	10.5190 nm	10.2281 nm	10.0942 nm	10.0854 nm
Standard Deviation of FWHM_x	2.7713 nm	2.0549 nm	1.3369 nm	0.6063 nm	0.5094 nm
Mean Value of FWHM_y	11.5260 nm	10.5202 nm	10.0681 nm	10.2531 nm	10.1980 nm
Standard Deviation of FWHM_y	2.3092 nm	1.9837 nm	1.0877 nm	0.8491 nm	0.4616 nm
Preset of height	1.5 nm	1.5 nm	1.5 nm	1.5 nm	1.5 nm
Mean Value of height	1.2244 nm	1.4326 nm	1.4884 nm	1.4620 nm	1.4781 nm
Standard Deviation of height	0.2338 nm	0.1720 nm	0.0908 nm	0.0788 nm	0.0544 nm
Generalized Error	16.69%	4.96%	1.37%	2.42%	1.43%

- Possible Solution:
  - Statistical averaging
  - Increase SNR √ √ (more hardware cost)

Demonstration: Size Estimation Results (different detector SNRs, ave. number = 30) (2/2)

Estimated width vs. increasing SNR

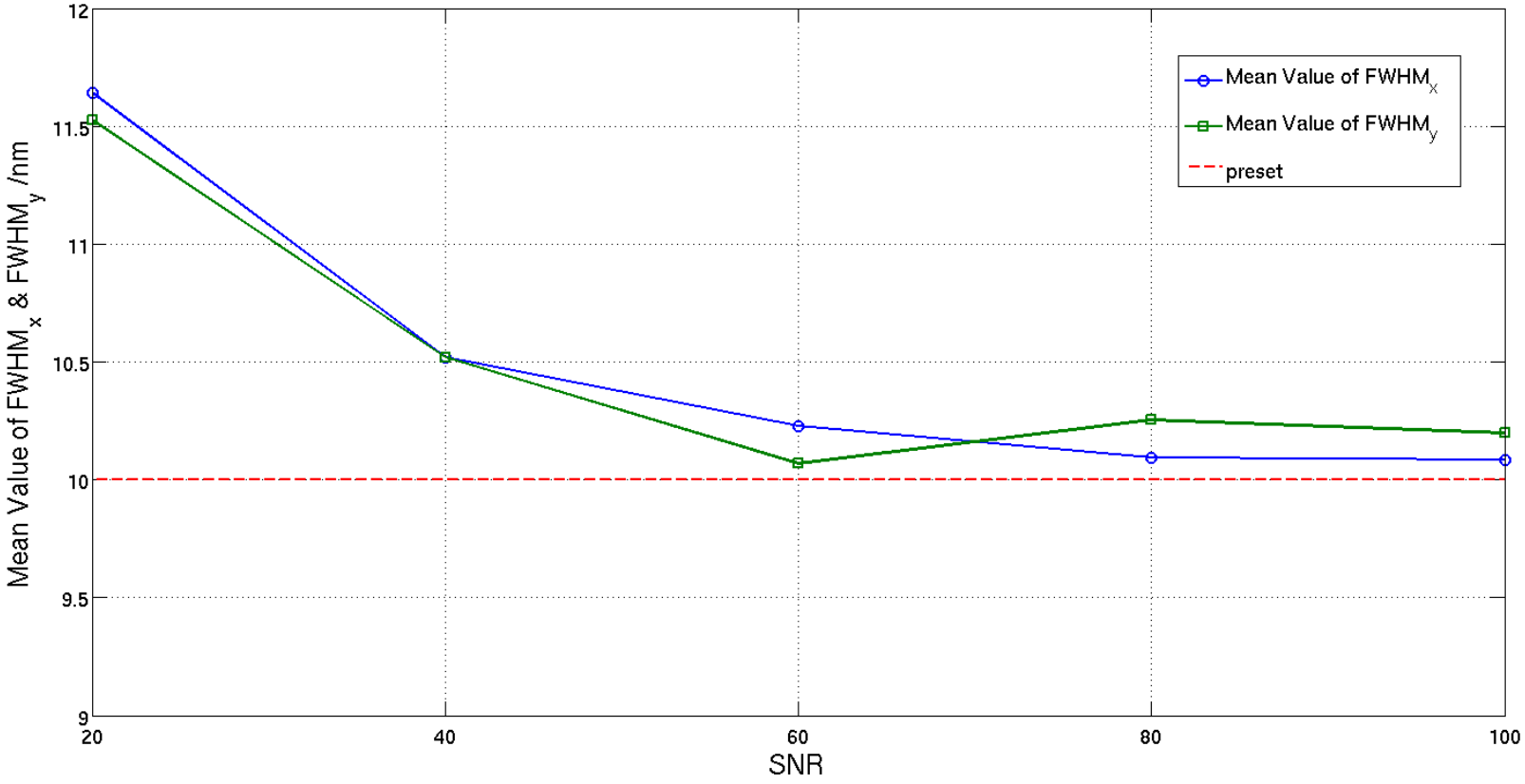

Demonstration: Size Estimation Results (different detector SNRs, ave. number = 30) (2/2)

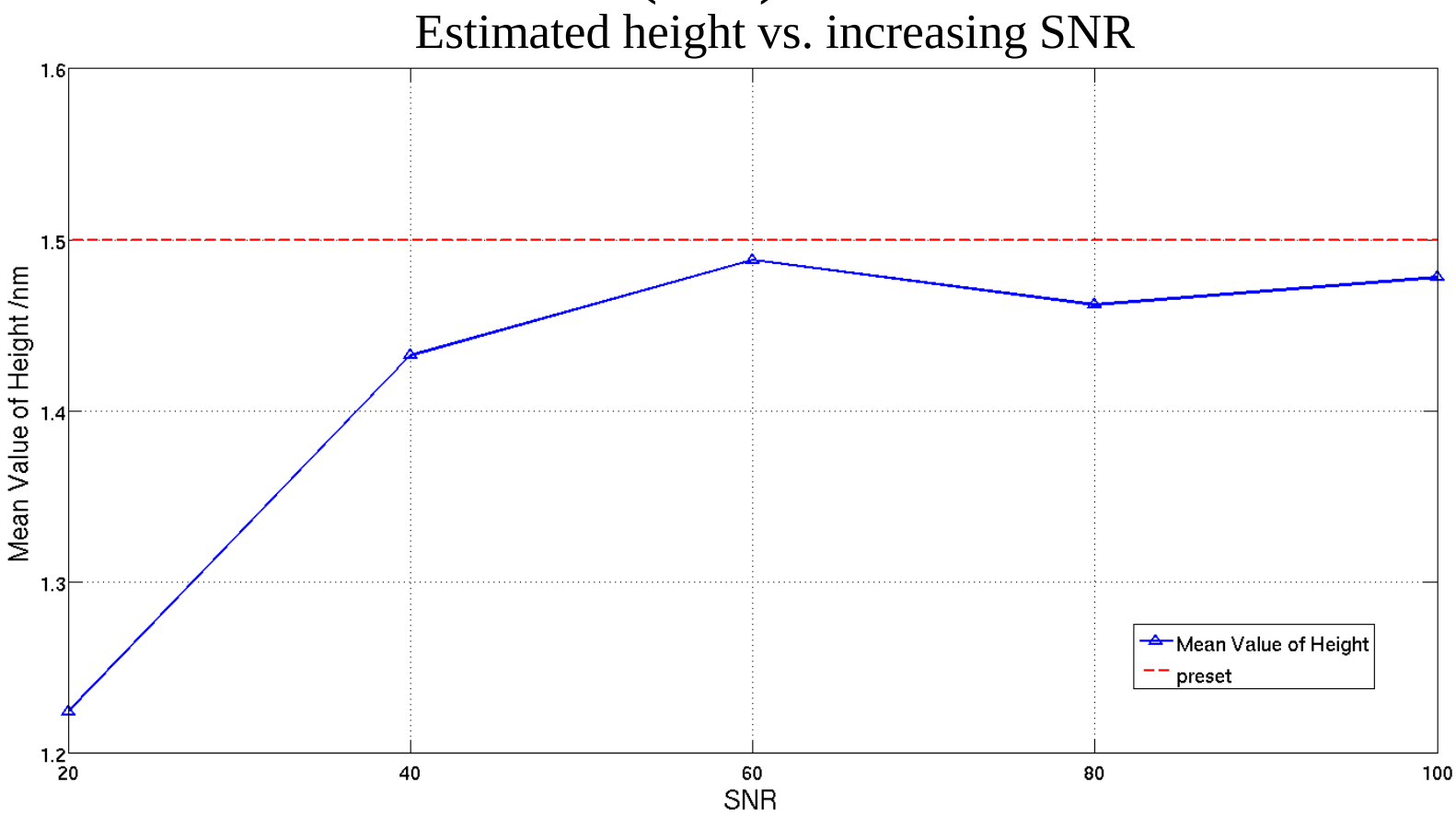

Defect Location Determination

- Fast scan and size estimation detects defect existence
  - Location uncertainty reduced from whole mask to within a beam spot area ($X_0 \pm 1/2\ R$, $Y_0 \pm 1/2\ R$)

- However, location determination within a beam spot (x_0, y_0) is difficult, if not impossible
  - Defect location shift results in phase shift of scattered light
  - Phase information lost in scattering intensity measurements
  - Exact location can be determined by other review tools (e.g., AFM, SEM, R = 1 μm adequate)

- *Relative* positions between *multiple* defects in a beam spot can be estimated
  - Locating one automatically reveals others' locations

Demonstration: Relative Position Estimation (2 defects)

Feature	Parameter	Preset
Defect1	FWHM_x	10 nm
	FWHM_y	10 nm
	Height	1.5 nm
Defect2	FWHM_x	8 nm
	FWHM_y	8 nm
	Height	1 nm
Relative position	Relative distance	100 nm
	Polar angle	60°

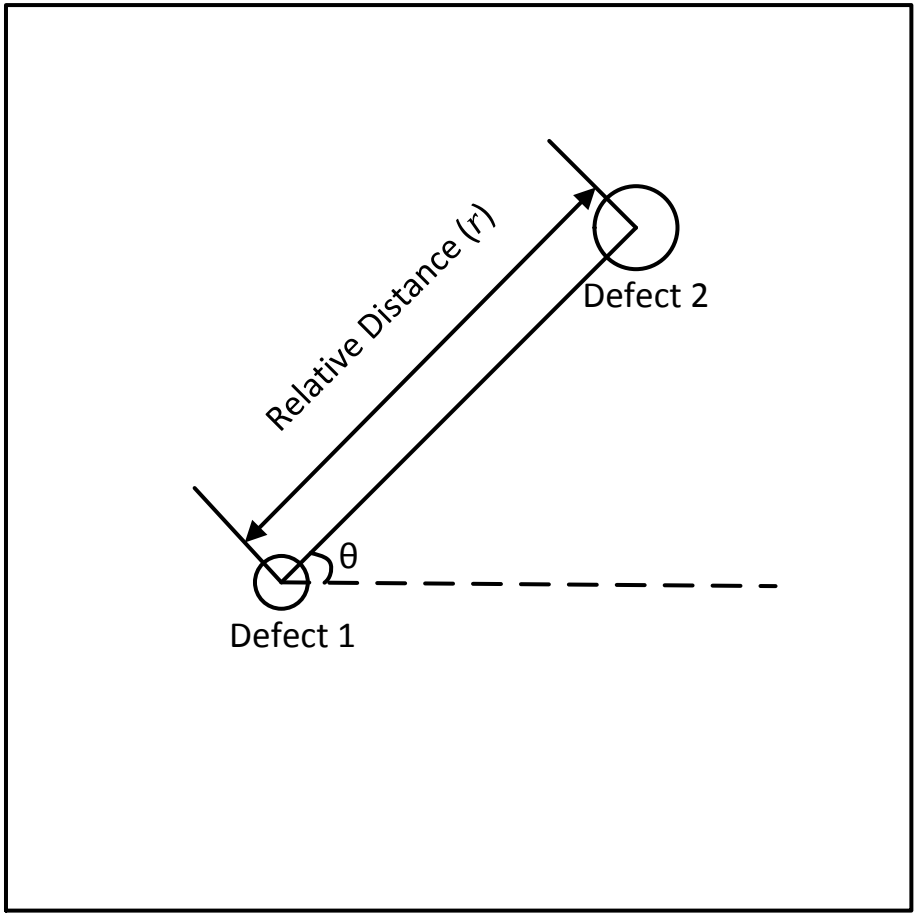

Metrology Window

Relative Position Estimation Results

Double Programmed Defect and Inspection Result

Group	Parameter	Target	Estimation rersult	Error
Defect1	FWHM_x	10 nm	10.72 nm	7.2%
	FWHM_y	10 nm	8.86 nm	11.4%
	Height	1.5 nm	1.63 nm	8.7%
Defect2	FWHM_x	8 nm	9.89 nm	23.6%
	FWHM_y	8 nm	12.75 nm	59.4%
	Height	1 nm	0.54 nm	46.0%
Relative Location	Relative distance	100 nm	99.7 nm	0.3%
	Polar angle	60°	59.63°	0.6%
Iteration			40	
Function Evaluation Number			776	
Computation Time			2.6 hour	

Finding: Relative location contributes to the diffraction signals the most among these feature parameters. Therefore, it can be well estimated.

Conclusion

- A non-imaging defection inspection method with non-imaging optics hardware
  - For the first time, both hardware and software complexity become quite manageable for high-resolution defect detection
- Zero-bias size estimation seems feasible
- Some level of detector noise resistance
- Location determination manageable by subsequent defect reviews
- Preliminary results indicate promising feasibility

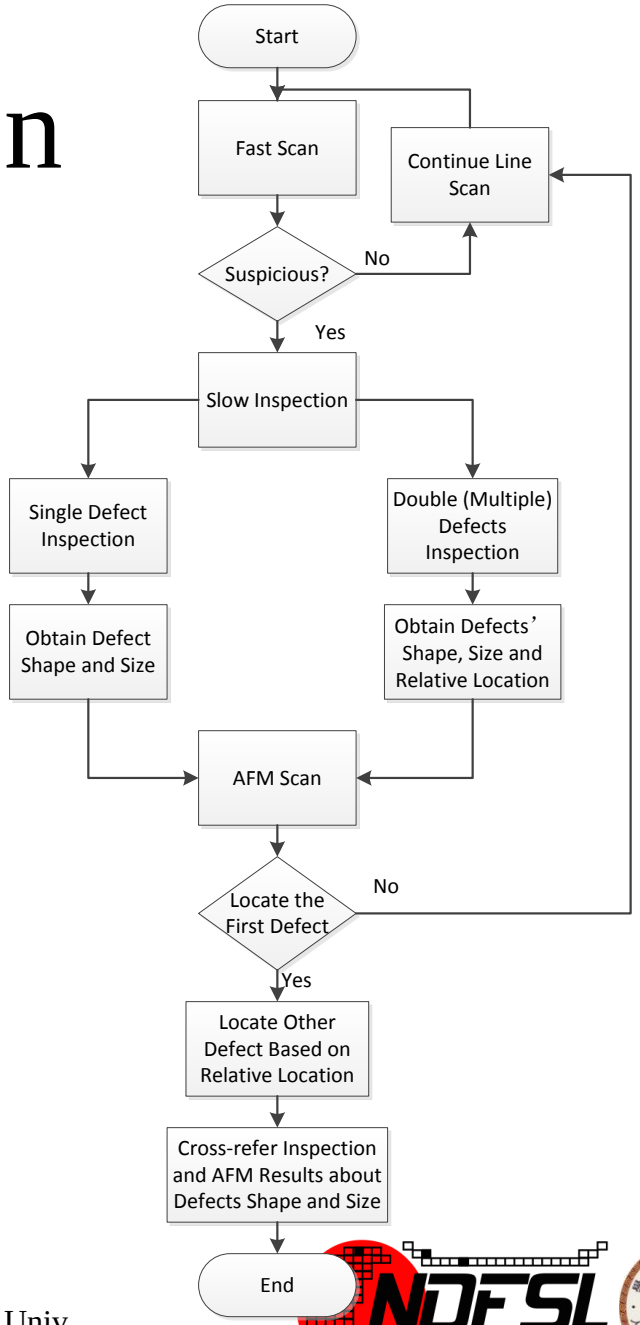

Reference

1. International Technology Roadmap for Semiconductors, http://public.itrs.net/.
2. M. Godwin, D. Balachandran, T. Tamura, A. Jia, “Comparative defect classifications and analysis of Lasertec's M1350 and M7360”, Proc. of SPIE Vol. 9050, 90502Z (2014).
3. K. A. Goldberg, A. Barty, P. Seidel, K, Edinger, R. Fettig, P. Kearney, H. Han, O. R. Wood II, “EUV and non-EUV inspection of reticle defect repair sites”, Proc. SPIE 6517, 65170C (2007)
4. K. A. Goldberg and I. Mochi, “Wavelength-specific reflections: A decade of extreme ultraviolet actinic mask inspection research”, J. Vac. Sci. Technol. B 28(6), C6E1-C6E10 (2010).
5. K. A. Goldberg, I. Mochi, M. P. Benk, C. Lin, A. Allezy, M. Dickinson, C. W. Cork, J. B. Macdougall, E. H. Anderson ; W. Chao, F. Salmassi, E. M. Gullikson, D. Zehm, V. Vytla, W. Cork, J. DePonte, G. Picchi, A. Pekedis, T. Katayanagi, M. S. Jones, E. Martin, P. P. Naulleau, S. B. Rekawa, “The SEMATECH high-NA actinic reticle review project (SHARP) EUV mask-imaging microscope”, Proc. SPIE 8880, 88800T (2013)
6. A. Tchikoulaeva, H. Miyai, T. Suzuki, K. Takehisa, H. Kusunose, T. Yamane, T. Terasawa, H. Watanabe, S. Inoue, I. Mori, “EUV actinic blank inspection: from prototype to production”, Proc. SPIE 8679, 86790I (2013)
7. S. Lee, M. Guizar-Sicairos, Y. Ekinci, “A novel concept for actinic EUV mask review tool using a scanning lensless imaging method at the Swiss Light Source”, Proc. SPIE 9048, 904811 (2014)
8. T. Harada, J. Kishimoto, T. Watanabe, H. Kinoshita, and D. G. Lee, “Mask observation results using a coherent extreme ultraviolet scattering microscope at NewSUBARU”, J. Vac. Sci. Technol. B 27(6), 3203-3207 (2009).
9. T. Harada, M. Nakasuji, T. Kimura, T. Watanabe, H. Kinoshita, and Y. Nagata, “Imaging of extreme-ultraviolet mask patterns using coherent extreme-ultraviolet scatterometry microscope based on coherent diffraction imaging”, J. Vac. Sci. Technol. B 29, 06F503 (2011).
10. T. Harada, M. Nakasuji, Y. Nagata, T. Watanabe, and H. Kinoshita, “Phase Imaging of Extreme-Ultraviolet Mask Using Coherent Extreme-Ultraviolet Scatterometry Microscope”, Jpn. J. Appl. Phys. **52**, 06GB02 (2013).
11. E. M. Gullikson, C. Cerjan, D. G. Stearns, P. B. Mirkarimi, and D. W. Sweeney, “A Practical approach for modeling extreme ultraviolet lithography mask defects”, J. Vac. Sci. Technol. B 20(1), 81-86 (2002).
12. I. Mochi, K. A. Goldberg, and S. Huh, “Actinic imaging and evaluation of phase structures on extreme ultraviolet lithography masks” J. Vac. Sci. Technol. B 28, C6E11 (2010).
13. A. Stivers, T. Liang, M. Penn, B. Lieberman, G. Shelden, J. Folta, C. Larson, P. Mirkarimi, C. Walton, E. Gulliksong and M. Yi, “Evaluation of the capability of a multibeam confocal inspection system for inspection of EUVL Mask Blanks”, Proc. of SPIE 4889, 408-417 (2002).
14. J.-P. Urbach, J. Cavelaars, H. Kusunose, T. Liang, and A. R. Stivers, “EUV substrate and blank inspection with confocal microscopy”, Proc. of SPIE 5256, 556-565 (2003).
15. E. M. Gullikson, E. Tejnil, K.-Y. Tsai, A. R. Stivers and H. Kusunose, “Modeling the defect inspection sensitivity of a confocal microscope”, Proc. of SPIE 5751, 1223-1229 (2005).
16. A. Barty, Y. Liu, and E. Gullikson, J. S. Taylor, and O. Wood, “Actinic inspection of multilayer defects on EUV masks”, Proc. of SPIE 5751, 651-659 (2005).
17. K.-Y. Tsai*; E. M. Gullikson, P. Kearney, and A. R. Stivers, “On the sensitivity improvement and cross-correlation methodology for confocal EUV mask blank defect inspection tool fleet,” 25th Annual BACUS Symposium on Photomask Technology -- Proc. of SPIE Vol. 5992, 599240, Monterey, California, USA, Oct. 2005